

Evaluation of high resolution snowpack simulations from global datasets and comparison with Sentinel-1 snow depth retrievals in the Sierra Nevada, USA

Laura Sourp^{1,2}, Simon Gascoin¹, Lionel Jarlan¹, Vanessa Pedinotti², Kat J. Bormann³, Mohammed Wassim Baba⁴

¹Centre d'Etudes Spatiales de la Biosphère, CESBIO, CNES/CNRS/INRAE/IRD/Université Toulouse 3 Paul Sabatier, 31401 Toulouse, France

²MAGELLIUM, Ramonville Saint-Agne, 31520, France

³Airborne Snow Observatories, Inc., Mammoth Lakes, CA, United States

⁴Science, Applications & Climate Department, European Space Agency, Frascati 00044, Italy

Correspondence to: L. Sourp (laurasourp@gmail.com)

Abstract. Spatial distribution of mountain snow water equivalent (SWE) is key information for water management. We implement a tool to simulate snowpack properties at high resolution (100 m) by using only global datasets of meteorology, land cover and elevation. The meteorological data are obtained from ERA5 which makes the method applicable in near real time (5 day latency). We evaluate the output using 49 SWE maps derived from airborne lidar surveys in the Sierra Nevada. We find a very good agreement at the catchment scale using uncalibrated lapse rates. Larger biases at the model grid scale are especially evident at high elevation but do not alter the catchment-scale snow mass accuracy. We additionally compare the simulated snow depth to Sentinel-1 retrievals and find a similar accuracy with respect to synchronous airborne lidar surveys. However, Sentinel-1 snow depth products are sparse and often masked during the melt season, whereas ERA5-SnowModel provides spatially and temporally continuous SWE.

1 Introduction

Many populated regions with dry summers and wet winters depend on mountain snow for water supply (Mankin et al., 2015; Sturm et al., 2017; Viviroli et al., 2020). Understanding the catchment scale seasonal snow storage before and during the melt season is key to optimizing water use between hydropower production, crop irrigation and freshwater supply. In addition, an accurate prediction of the timing and magnitude of the snowmelt runoff is bound by our ability to characterize the spatial distribution of mountain snow before the melt season (Freudiger et al., 2017).

28 Despite its hydrological significance, the snow water equivalent (SWE) remains poorly monitored in many mountain regions
29 especially outside North America and Europe. In situ measurements are often too sparse considering the spatial variability of
30 mountain snow (Fayad et al., 2017). To cope with this issue, airborne measurement campaigns are now routinely used in the
31 western USA to measure snow depth but their cost remains prohibitive in other regions (Painter et al., 2016). Meanwhile,
32 several approaches have emerged to retrieve mountain snow depth from satellite remote sensing (e.g. Pléiades, ICESat-2 and
33 Sentinel-1). Pléiades is limited to small regions (Marti et al., 2016), while ICESat-2 provides only sparse sampling (Deschamps-
34 Berger et al., 2023). Sentinel-1 has been used to derive snow depth at 1 km resolution in the northern hemisphere (Lievens et
35 al., 2019), and 500 m over the European Alps (Lievens et al., 2022). This method is limited to dry snow conditions and therefore
36 does not allow monitoring of the snowpack during the melt season. However, it offers a global and spatially continuous
37 coverage which is a key advantage with respect to the other approaches. All the above remote sensing approaches require an
38 estimation of snow density to obtain the SWE, but it has been established that snow depth explains most of the SWE variance
39 (Guyennon et al., 2019; López-Moreno et al., 2013; Sturm et al., 2010; Bormann et al., 2013).

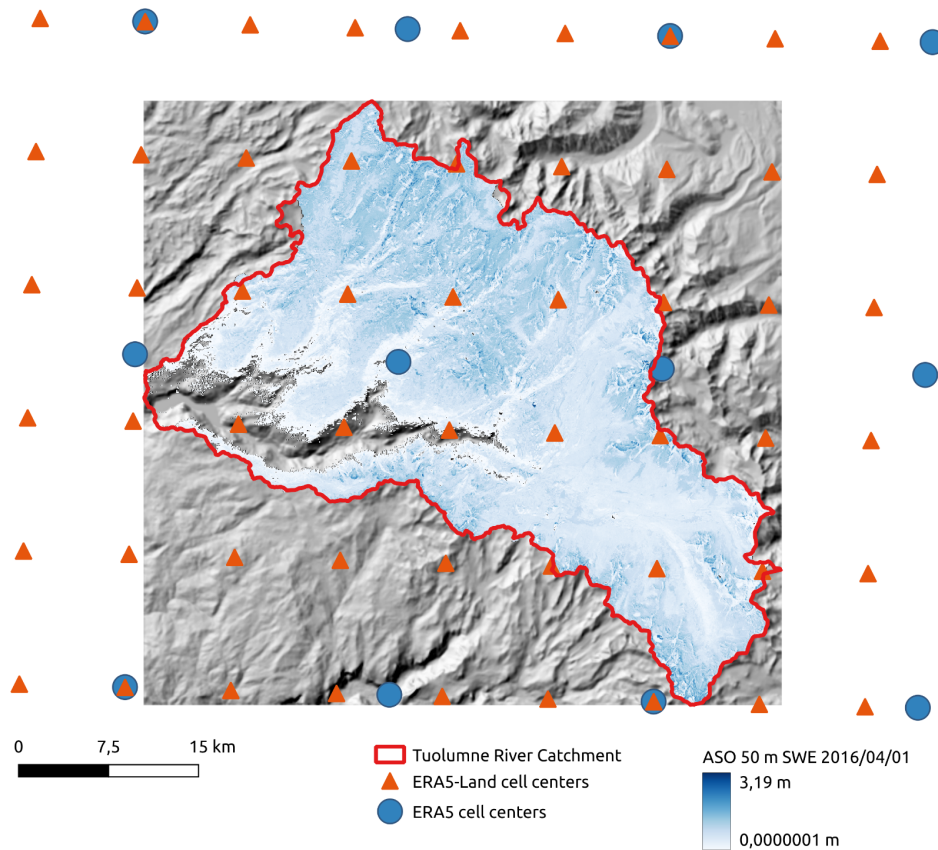
40
41 Another approach to estimating mountain SWE distribution is to use a snowpack model, but the challenge then lies with
42 obtaining accurate meteorological forcing (Günther et al., 2019; Raleigh et al., 2016). To cope with the lack or sparsity of in
43 situ meteorological measurements, one solution is to use atmospheric model outputs as forcing data. In particular, climate
44 reanalyses can provide long term hourly meteorological data at global scale. Climate reanalyses are also becoming increasingly
45 accurate (Hersbach et al., 2020) with advances in atmospheric and land surface modeling and the assimilation of a growing
46 dataset of in situ and remote sensing observations. These reanalyses have also seen notable progress in recent years in terms
47 of latency. For example, the preliminary ERA5 reanalysis provided by the European Centre for Medium-Range Weather
48 Forecasts has a short latency of 5 days (whereas it was 2–3 months with the previous ERA-Interim). This preliminary product
49 only rarely deviates from the fully quality-checked final product that is released 2 months later (Hersbach et al., 2020). This
50 timely product can fulfill the need for up-to-date meteorological forcing information. However, reanalyses cannot be used
51 directly to force a mountain snowpack model because the grid cell size is too coarse (approximately 30 - 50 kilometers for
52 ERA5 and MERRA-2 respectively), which creates large biases in the computed SWE (Wrzesien et al., 2019; Liu et al., 2022).

53
54 To address the mismatch in spatial resolution between reanalyses datasets and snow distribution, previous studies used
55 downscaling algorithms based on a digital elevation model before running a snowpack model on a finer grid (Armstrong et al.,
56 2018; Baba et al., 2018; Billecocq et al., 2023; Mernild et al., 2017; Weber et al., 2021). This approach enables estimation of
57 high resolution SWE and snow depth without ground data. For example, Mernild et al. (2017) and Baba et al. (2018) studied
58 the snowpack properties over large and ungauged regions in the Andes and the High Atlas mountain ranges using the
59 MicroMet/SnowModel package (Liston et al., 2020; Liston and Elder, 2006a, b). The evaluation of these simulations relied on
60 in situ observations or remote sensing snow cover area. Weber et al. (2021) used 10 years of snow depth measurements from
61 two automatic weather stations to assess their simulations in the Research Catchment Zugspitze (12 km²). Mernild et al. (2017)

62 used 13 years of MODIS data over the Andes Cordillera (~16 million km²) along with 4 km grid maps of snow depth that were
63 reconstructed from in situ observations. Baba et al. (2018) used 18 years of MODIS data to assess simulations in the High
64 Atlas of Morocco, snow depth at a single automatic weather station, precipitation at three meteorological stations and river
65 discharge of the Ourika catchment (503 km²). However, in situ data are sparse and MODIS snow cover area does not allow a
66 thorough evaluation of the model ability to capture snow mass across the landscape.

67
68 In this study, we focus on the Tuolumne River catchment in the Sierra Nevada, USA (Figure 1). Since 2013, this site has been
69 regularly surveyed by the Airborne Snow Observatory (ASO) to determine snow depth and SWE. The ASO Tuolumne dataset
70 is the densest time series of high resolution snow depth (3 m) and SWE (50m) maps available worldwide at this scale
71 (1100 km²). The dataset contains 49 surveys and spans several years with contrasted climatic conditions including California's
72 most severe drought in the last 1200 years during 2012-2014 (Griffin & Anchukaitis, 2014) and the "snowpocalypse" 2016–
73 2017 winter which was characterized by near-record snow accumulation (Painter et al., 2017). We leverage this observational
74 dataset to evaluate a new processing pipeline which generates 100 m resolution SWE and snow depth estimates from ERA5
75 or ERA5-Land. This pipeline, inspired by previous works (Baba et al., 2018; Mernild et al., 2017) is a wrapper around
76 MicroMet/SnowModel code. It was designed to work with global meteorological forcing datasets. As such, the workflow can
77 generate high resolution snow cover simulations in any region of interest across the globe from 1940 up to present, with any
78 resolution between 1 m and 200 m (Liston and Elder, 2006b). Furthermore, we compare the output of this pipeline with the
79 more direct approach of Sentinel-1 snow depth on dates matching the ASO measurements.

80



81

82 **Figure 1: Map representing the SWE variability measured by ASO, along with ERA5 and ERA5-Land cells centers**
 83 **and the Tuolumne River catchment border overlaying the DEM hillshade.**

84 **2 Data and Methods**

85 **2.1 Data**

86 We used two reanalyses in this study, ERA5 and ERA5-Land. ERA5 is a reanalysis of the global climate and weather since
 87 1940, with a 0.25° resolution (approximately 30 km). It provides hourly atmospheric, oceanic and land-surface variables
 88 computed with a global model and improved by the assimilation of multiple in situ and remote sensing datasets (Hersbach et
 89 al., 2020). ERA5-Land is produced by recomputing ERA5 land variables at finer resolution using a downscaled meteorological
 90 forcing (Muñoz Sabater, 2019). It delivers these variables on a global scale at a 0.1° resolution, from 1950 to this day. As
 91 mentioned above, preliminary versions of ERA5 and ERA5-Land are distributed with a short latency of 5 days. These datasets
 92 are freely available from the Copernicus Climate Change Service (C3S) and can be queried via their application programming
 93 interface (with tutorials that can be found on their website : Retrieving data — Climate Data Store Toolbox 1.1.5
 94 documentation)

95 . We focused on ERA5 here as we found that it yielded slightly better results than MERRA-2 in a previous case study using
96 the same approach (Baba et al., 2021). In addition, the latency of MERRA-2 is 3 weeks which may be too long for operational
97 water resources applications. To run the model (see below), we also used the 30 m Copernicus Digital Elevation Model (DEM)
98 (Copernicus Digital Elevation Model, 2023) and the 100 m Copernicus Land Cover (Buchhorn et al., 2020).

99

100 We obtained Sentinel-1 snow depth between 2016 and 2019 from the C-SNOW repository. Sentinel-1 C-band backscatter
101 observations were used to derive ~1 km resolution snow depth, using an empirical change detection (Lievens et al., 2019).
102 This product has a revisit time of approximately 3 days over the Tuolumne River catchment during winter but provides almost
103 no data in spring because the algorithm is considered to be invalid when the snowpack contains liquid water. When the
104 snowpack is wet, there is a larger absorption and reflection of the microwave signal emitted by Sentinel-1 which greatly
105 decreases the performances of the C-SNOW algorithm (Lievens et al., 2019; Tsai et al., 2019)

106

107 For the evaluation of model outputs and Sentinel-1 products, we used 49 SWE and snow depth maps collected between 2013
108 and 2019 by the ASO. The ASO acquires hyperspectral data for snow albedo and lidar data for snow depth and computes SWE
109 as a derived product (Painter et al., 2016). Snow depth is available with a 3 m resolution while SWE has 50 m resolution. The
110 reported accuracy on the 3 m snow depth products is 0.08 m (Painter et al., 2016) and from spatially intensive sampling, the
111 reported accuracy for the 50m snow depth products is < 0.01 m (Painter et al., 2016, Figure 15). There are no published
112 references for the 50 m SWE product. However, for a 1 m deep snowpack and a conservative 10% uncertainty in snow density
113 (20-50 kg/m³), we estimate the uncertainty of the 50 m SWE products to be 0.02 - 0.05 m w.e.

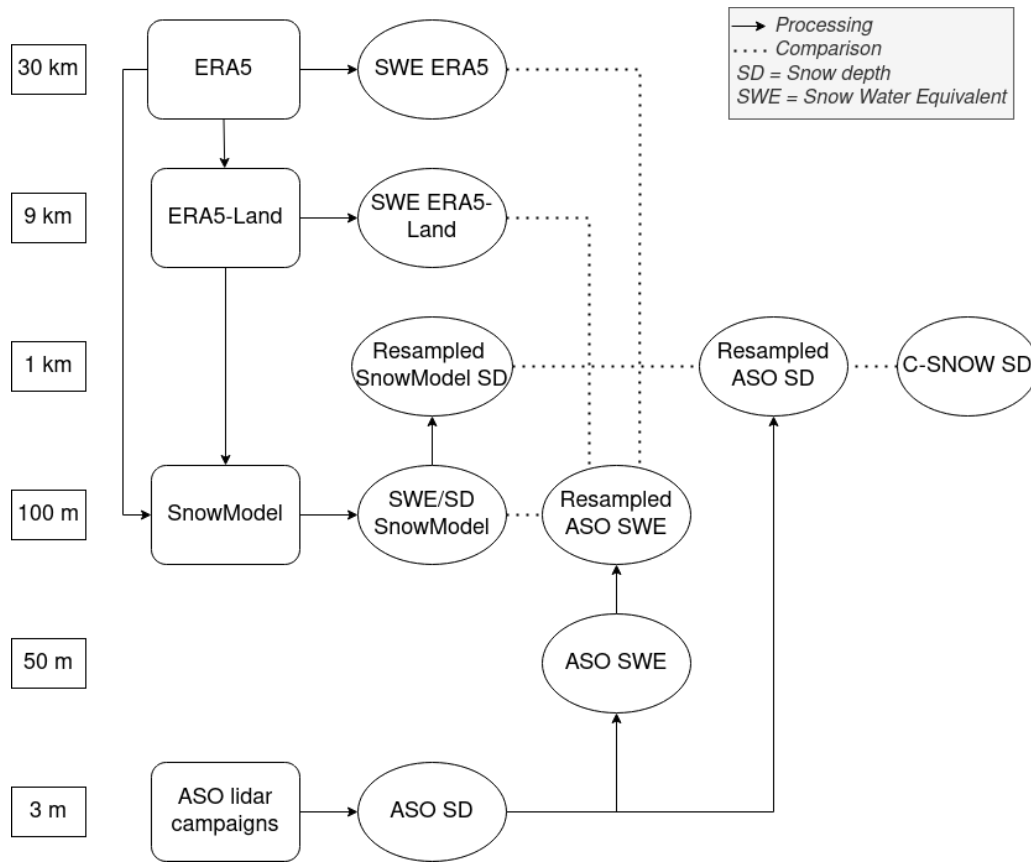
114 **2.2 Methods**

115 **2.2.1 SnowModel**

116 SnowModel is designed to simulate snow evolution on a high resolution grid (1 m to 200 m increments) and a time step from
117 1 min to 1 day (Liston et al., 2020; Liston and Elder, 2006a). It is separated into four submodels: i) MicroMet redistributes
118 meteorological forcings (air temperature, relative humidity, wind speed and direction, precipitation, solar radiation, long wave
119 radiation, and surface pressure) to the target simulation grid (Liston and Elder, 2006b). ii) EnBal computes the snow surface
120 energy balance, iii) SnowPack computes the snow density and snow depth and iv) SnowTran-3D computes the blowing snow
121 sublimation and snow redistribution due to wind transport (Liston et al., 2007). SnowModel accounts for the vegetation effects
122 on the snow cover such as coniferous forests or grassland to the grid cell vegetation type. MicroMet was originally designed
123 to interpolate station data on a regular grid. Here, a climate reanalysis grid cell is considered as a virtual station located at the
124 grid cell center.

125

126 **2.2.2 Model input**



127

128 **Figure 2: Summary of the different data sources, with their spatial resolutions. Arrows represent a process and the**
 129 **dotted lines the comparison between different data.**

130

131 We developed a tool to automatically prepare SnowModel input files from ERA5 and ERA5-Land data and run the simulations.
 132 This tool uses a digital elevation model (DEM) of the region of interest as an input along with the start and end of the simulation
 133 period. We let the user specify the DEM because it is used to define the model grid, which is the main control of the
 134 computation time. Here we used the 30 m Copernicus orthometric DEM that we extracted and resampled to a WGS84 UTM
 135 11N grid at 100 m resolution using the bilinear method over a region covering the Tuolumne River catchment. The simulation
 136 period was set to September 2012-August 2019, and spans seven years of snowpack dynamics. Using the Climate Data Store
 137 Application Program Interface, our tool downloads ERA5 or ERA5-Land hourly meteorological data (2 m temperature, 2 m
 138 dew point temperature, precipitation, 10 m wind eastward and northward component) over the region of interest given by the
 139 DEM bounding box extended to the adjacent ERA5/ERA5-Land neighbouring cells (~30km/11km respectively). Once
 140 downloaded, the meteorological data are processed to match SnowModel/MicroMet input format and

141 units. ERA5-Land precipitation is provided as daily cumulative values and is therefore converted to hourly precipitation rate.
142 Wind components (u,v) are converted into wind speed and direction (0-360°N). The dew point temperature is converted into
143 relative humidity using Buck's equation (Buck, 1981), the same equation that is used in MicroMet. The elevations of
144 ERA5/ERA5-Land cells are determined from the global geopotential file that is first interpolated on the model grid with a
145 bilinear algorithm. The tool also resamples the Copernicus land cover map on the model grid using the mode resampling
146 algorithm (GDAL/OGR contributors, 2024). We built a correspondence table to remap the Copernicus land cover classes to
147 the SnowModel land cover classification (see Table A1 in appendix). We set all SnowModel parameters (the curvature length
148 scale, curvature and wind slope weights, minimum wind speed, precipitations schemes for downscaling or for rain-snow
149 fractions, subcanopy radiations schemes, various thresholds for wind transport calculations) to the default values. A simple
150 parametrization of the albedo is used with a constant value 0.8 in dry condition, whereas albedo values for melting snow cover
151 are set according to land covers (Liston et al., 2020). We used the default monthly temperature lapse rates and precipitation
152 factors which adjust the precipitation values to the elevation of the model grid. This tool is implemented in Python. The source
153 code and a more detailed documentation is available at (code availability section).

154 **2.2.3 Comparison with ASO SWE**

155 We resampled the ASO SWE (n=49 surveys) to the model grid which has a resolution (100 m). The resampling was done
156 using the weighted average of all valid contributing pixels (GDAL/OGR contributors, 2024). We also created a validity mask
157 to select cells in the Tuolumne River catchment that were always observed by the ASO during this period (some regions were
158 not always available, representing 2.5% of the catchment area). ASO data and ERA-SnowModel outputs were averaged over
159 the valid cells to compute the temporal evolution of the catchment-mean SWE. Then, we analyzed the spatially distributed
160 residuals on the catchment for each observation date of a dry year (2014-2015), a wet year (2016-2017) and an average year
161 (2015-2016). We used the validity-masked SWE maps to subtract the ASO observations from the ERA-SnowModel output. A
162 positive bias means the simulated SWE is larger than the observations.

163
164 Additionally, we extracted ERA5 and ERA5-Land daily SWE over the Tuolumne River catchment and computed the
165 catchment scale SWE using an area weighted average (i.e. each SWE value was weighted by the fraction of the grid cell area
166 within the catchment). Since these SWE products have a very coarse resolution of approximately 31 and 9 km (Fig. 1, Fig. 2),
167 we did not use them to analyze the residuals distribution as above.

168 **2.2.4 Comparison with Sentinel-1 snow depth**

169 Over the entire study period, we identified three matchup dates for which we have both ASO and Sentinel-1 snow depth
170 observations with a minimum coverage of 60% of the catchment area. On these dates, the snow depths given by ASO, Sentinel-
171 1 and ERA-SnowModel were resampled to a common 1 km UTM grid. We applied another validity mask for the cells where
172 the snow depth is not always available to all three snow depth datasets (here representing 8.5% of missing data in the

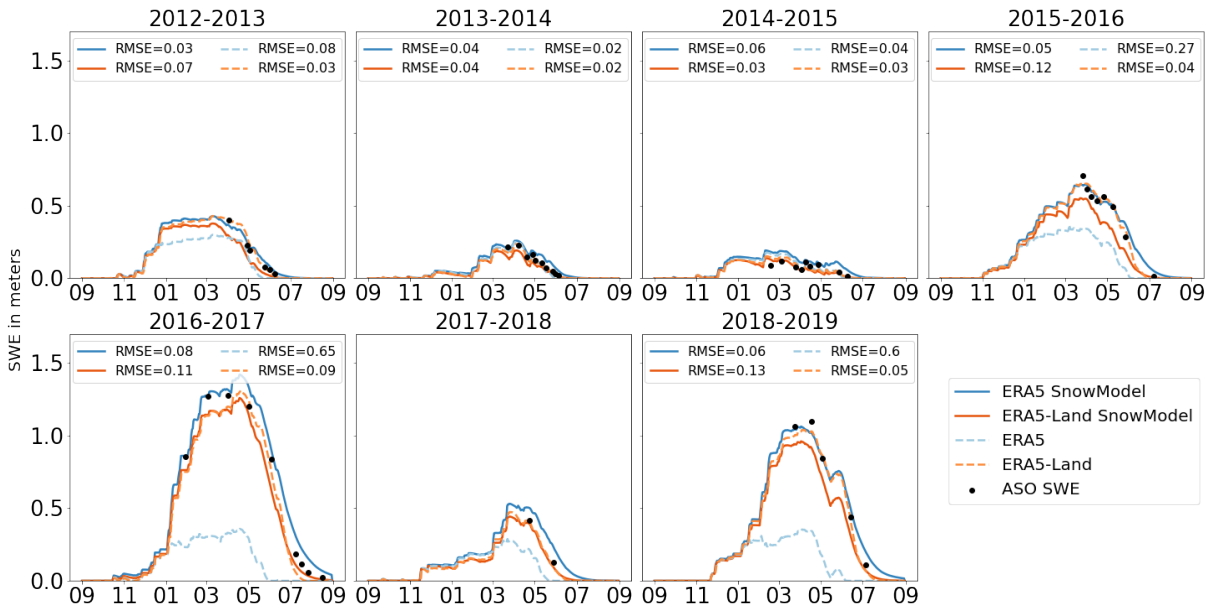
173 catchment). We computed the distributed residuals by subtracting the ASO snow depth from both SnowModel simulations and
174 Sentinel-1 data. For each date, we averaged the residuals to compute the mean bias, and we computed the standard deviation
175 of the error. We also computed the RMSE over the catchment for each date .

176 **3 Results**

177 **3.1 Comparison with ASO SWE**

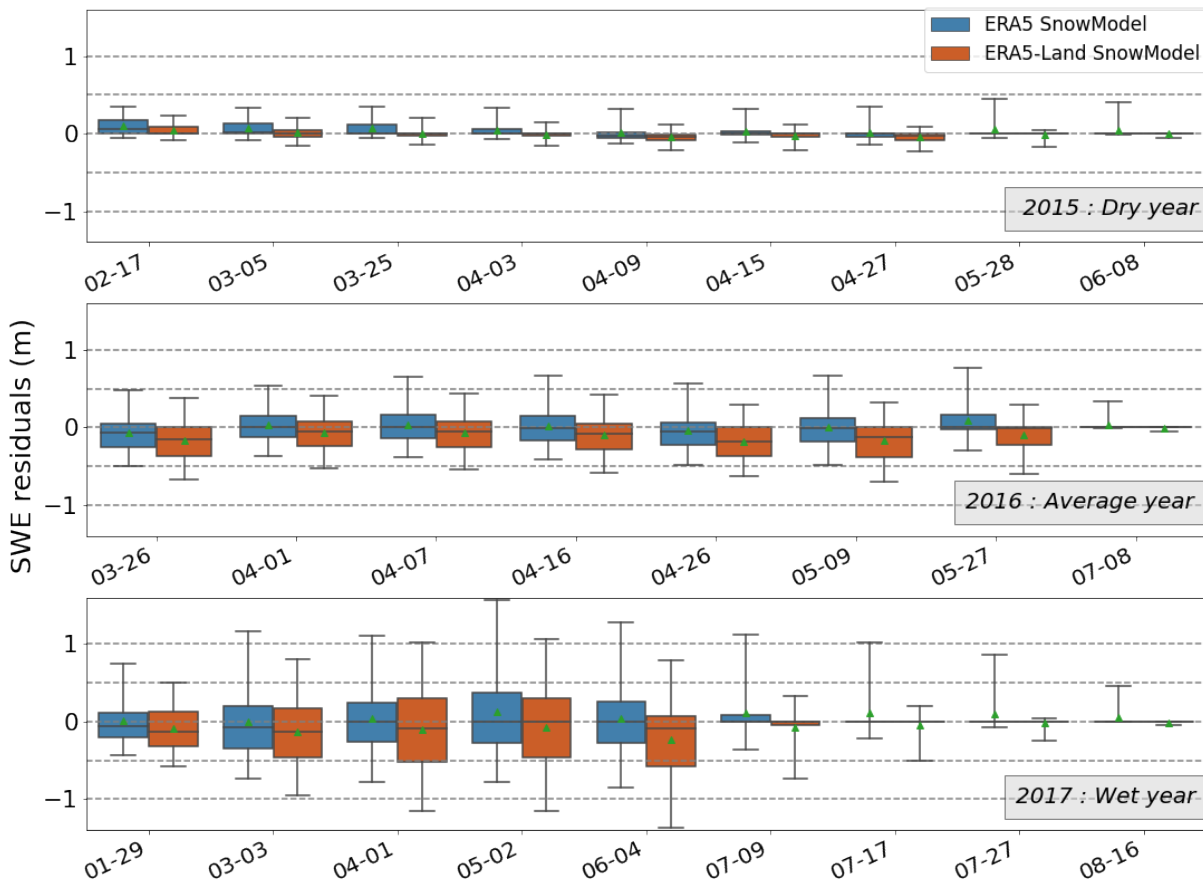
178 Figure 3 shows the temporal evolution of the catchment scale SWE from ASO observations and SnowModel simulations
179 forced with ERA5 and ERA5-Land. There is a very good agreement between the observations and both simulations, with an
180 overall correlation of 0.99 for both ERA5 and ERA5-Land SnowModel simulations (with 49 observation dates). First, both
181 simulations capture the large interannual variability of SWE in the Tuolumne River catchment during the study period. The
182 observed annual peak SWE ranges from 0.11 m in 2015 to 1.27 m in 2017 while the SnowModel simulations yield from 0.17
183 m to 1.19 m with ERA5 and from 0.12 m to 1.24 m with ERA5-Land during the same years (but at different dates). In addition,
184 the model is reproducing the seasonal evolution of SWE with an annual RMSE ranging from 0.03 m to 0.13 m. The catchment
185 scale SWE accumulation in the ERA5-SnowModel simulations is well captured. We note an underestimation of the snow
186 ablation rates in late spring, which causing a delay from a few days (2013) to one month approximately (2019) in the date of
187 complete melt out. This issue is mostly evident in 2016-2017 since the ablation rates are insufficient to reach the complete
188 removal of the snowpack in August as observed by the ASO. Interestingly, we also note that ERA5-Land without resampling
189 almost always reports the lowest RMSE at the catchment scale, though at 0.1° the distribution of the snow is not well
190 represented.

191



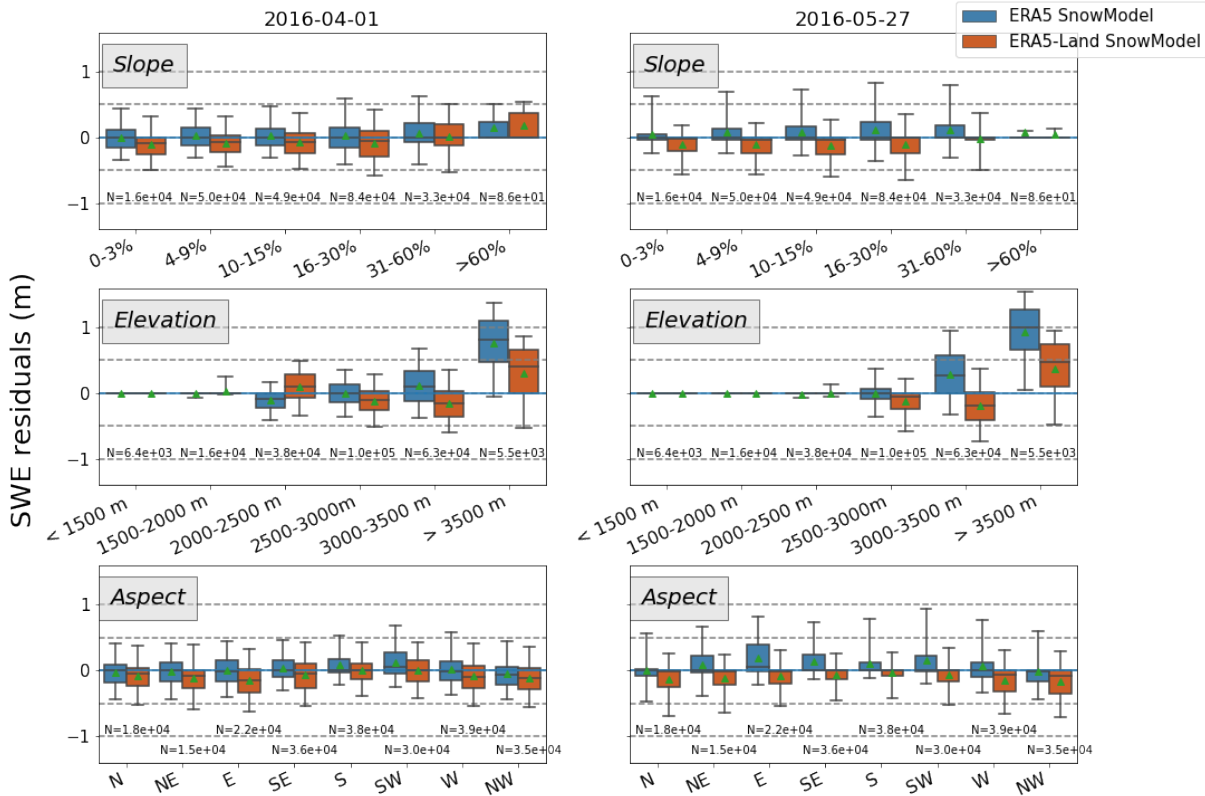
192
193 **Figure 3: Temporal evolution of the Tuolumne river catchment SWE for seven hydrological years from 2012 to 2019.**
194 **The legend indicates the RMSE between the simulated SWE and the ASO SWE for each year.**

195
196 To go beyond this coarse catchment scale diagnostic (1100 km²), we also analyze the distribution of the residuals at the pixel
197 scale (0.01 km²). We computed a map of RMSE using all the 49 validation dates we have between 2013 and 2019. 10% of the
198 cells in this map have a RMSE above 0.5 m w.e.. Figure 4 shows the distribution of the residuals for every date with ASO
199 observations for three contrasted hydrological years. This figure indicates that the spread of the residuals increases with the
200 mean SWE depth. For the dry year, the interquartiles of SnowModel SWE residuals for ERA5 and ERA5-Land do not exceed
201 0.17 m and 0.09 m w.e. respectively. For the average year, the interquartiles reach 0.31 m and 0.38 m w.e. and for the wet
202 year 2017, they peak respectively at 0.64 and 0.82 m w.e.



204
 205 **Figure 4: Distribution of the residuals between the SnowModel simulated SWE and the ASO SWE at 100 m resolution**
 206 **in the Tuolumne river catchment (in m w.e.) for three contrasted hydrological years. Filled boxes represent the**
 207 **interquartile range, the whiskers show the 5-95 percentiles, the line in each box represents the median of the**
 208 **distribution, and the green triangle shows the mean.**

209
 210 Figure 5 shows the distribution of the residuals for two dates by slope, elevation and aspect. We aimed to distinguish the model
 211 performance in terms of accumulation and ablation processes to better separate the sources of uncertainties in future studies.
 212 Therefore we selected a date before the melting season (April 01) and a date near the end of the melting season (May 27).. The
 213 interquartile of the error distribution never exceeds 0.41 m.w.e. in slope or aspect categories but peaks at 0.67 m.w.e. in the
 214 highest elevation band the 1st of April for the simulations forced with ERA5-Land.



216

217 **Figure 5: Distribution of the residuals between the SnowModel simulated SWE and the ASO SWE at 100 m resolution**
 218 **in the Tuolumne river catchment (in m w.e.) on the 1st of April 2016 and the 27th of May, stratified by slope (in percent),**
 219 **elevation (in m a.s.l.) and aspect (in degrees from north). Whiskers show the 5-95 percentile, the line in each box**
 220 **represents the median of the distribution and the green triangle shows the mean. Slope, elevation and aspects have been**
 221 **calculated using the DEM at 100 m resolution.**

222 **3.2 Comparison with Sentinel-1 snow depth**

223 Between 2016 and 2019, there are three dates for which we have both Sentinel-1 and ASO snow depth data. Figure 6 presents
 224 snow depth maps on the Tuolumne River catchment at 1 km resolution with Sentinel-1, ASO and ERA5-SnowModel data.
 225 Some pixels are not always observed with ASO data and these missing values are propagated at 1 km resolution (if there is at
 226 least one missing value among the contributing pixels, a missing value is attributed to the target 1 km cell). The same mask is
 227 applied on the SnowModel simulations and Sentinel-1 data. Additional missing values are observed in the Sentinel-1 snow
 228 depth maps. Therefore, the statistics of Figure 7 are not computed on the exact same area. We chose to take all possible data
 229 into account.

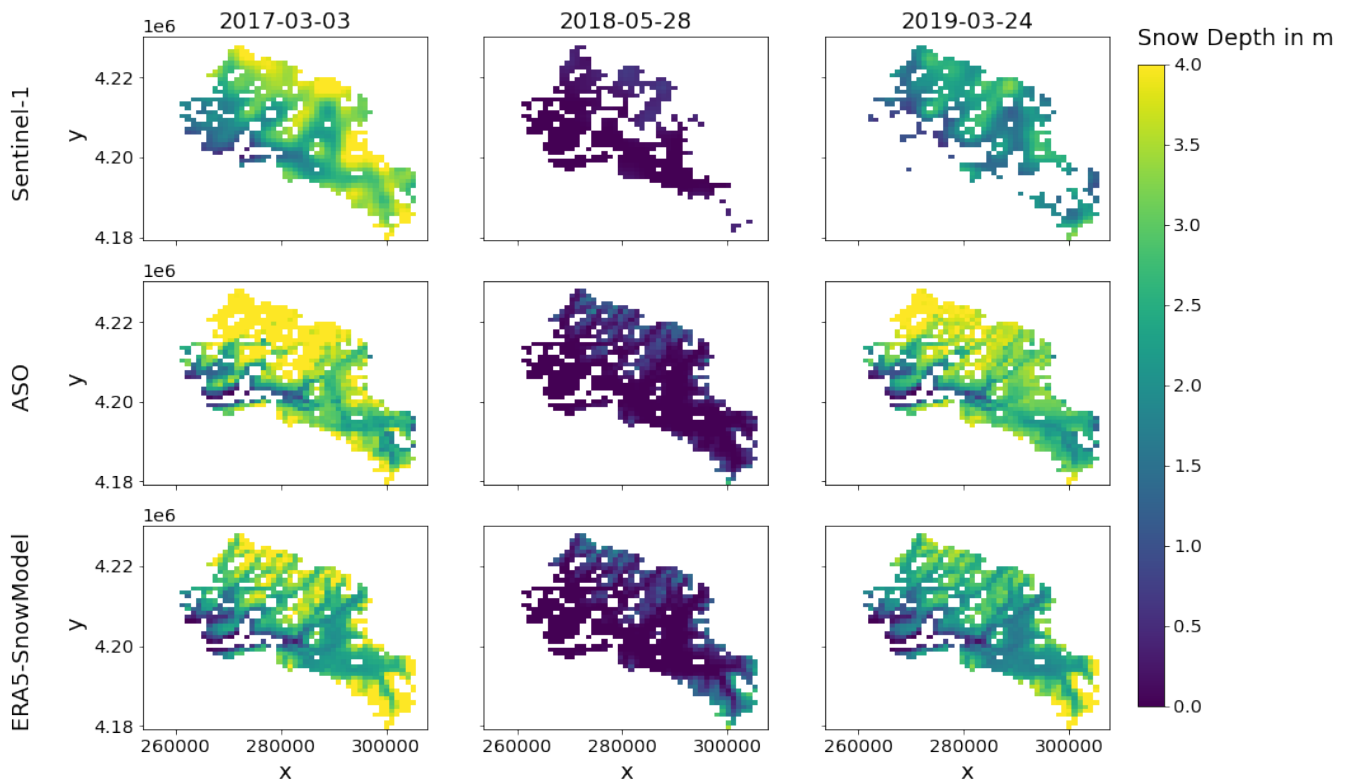
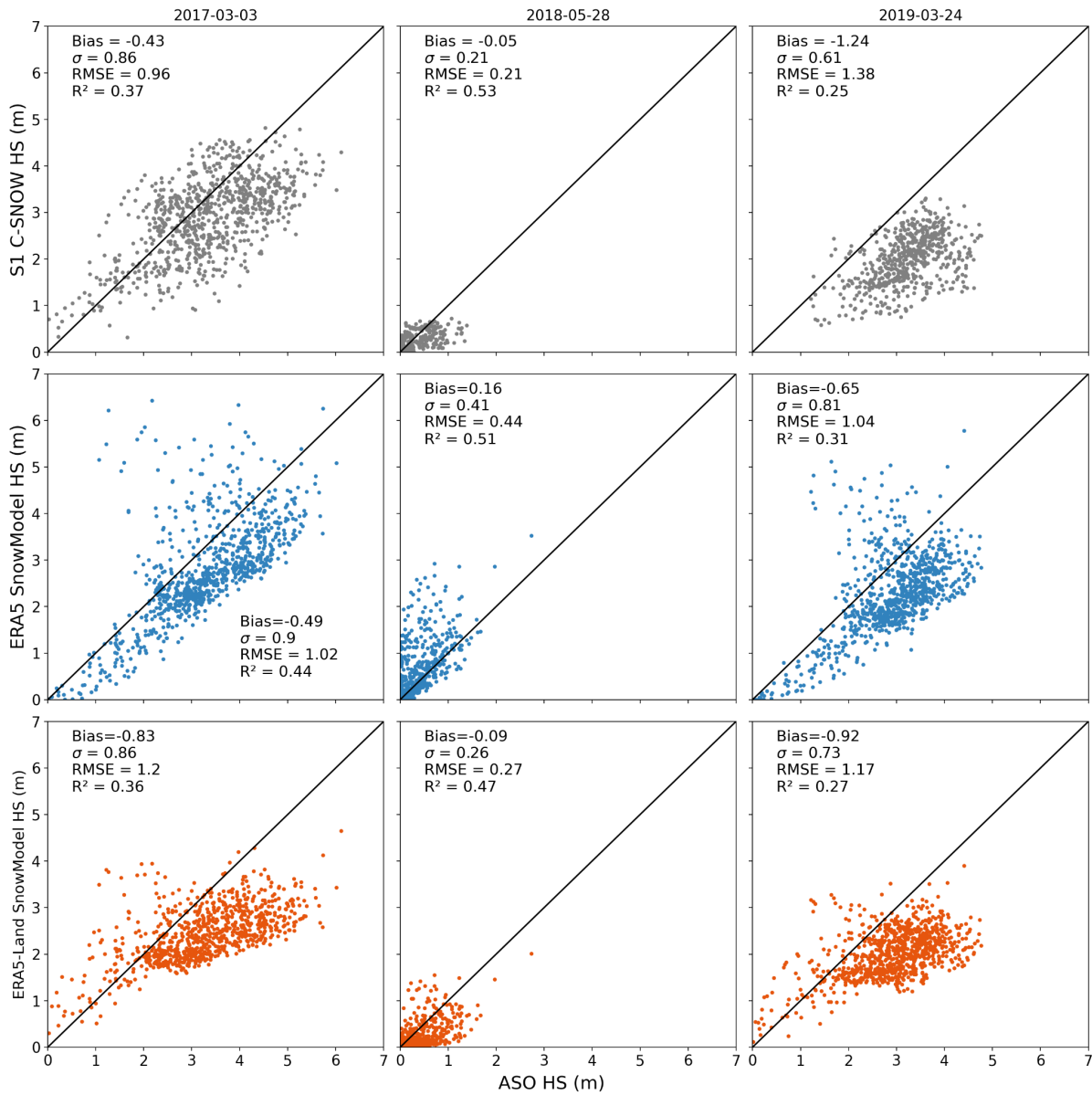


Figure 6: Snow depth maps at 1 km resolution with Sentinel-1, ASO and ERA-SnowModel data.

Figure 7 shows the Sentinel-1 observed and SnowModel simulated snow depth compared to the ASO observed snow depth, resampled to a 1 km resolution. On the 2017-03-03, Sentinel-1 has the lower bias, standard deviation and RMSE, not far from the ERA5-SnowModel simulations while ERA5-Land-SnowModel simulations have a greater bias and RMSE. On the second date, the 2018-05-01, Sentinel-1 still performs the best, followed this time by ERA5-Land-SnowModel simulations while ERA5-SnowModel simulations underperform. Finally on the 2019-03-24, the closer data to the ASO snow depths seems to be the ERA5-SnowModel simulations and Sentinel-1 data have the most unsatisfactory performance. We see an underestimation of the snow depth above 2 meters with Sentinel-1 in 2017 and 2019, which is very clear for 2019 when the mean bias is the highest with a relatively low standard deviation. In 2018, Sentinel-1 also underestimates the snow depth. With the ERA5 SnowModel simulations, most of the distribution is centered around a mean bias that is underestimating the snow depth in 2017 and 2019. We note several cells with a high positive error. In 2018, the situation is reversed : most of the snow depth estimated with ERA5 SnowModel are overestimated. Finally, the simulations with ERA5-Land seem to cap at 4 meters of snow depth in 2017 and 2019, with a declining accuracy with the ASO snow depth starting at 2 m. In 2018, the ERA5-Land SnowModel simulations are mostly underestimating snow depths.



247

248

Figure 7: Scatter plots representing the observed and SnowModel simulated snow depth data as a function of ASO snow depth data, with a one to one line in black. All data are resampled at 1 km resolution.

249

250

251

4 Discussion

252

253 Downscaling ERA5 forcing is critical to obtain realistic SWE in the Tuolumne catchment and is sufficient to remove the strong
254 negative bias that is otherwise present in the original ERA5 SWE (Fig 3). The use of this pipeline for long simulation periods
255 could also bypass the discontinuities in the ERA5 SWE (Urraca and Gobron, 2023) which are caused by a snow capping in
256 the data assimilation code and the arrival of new snow depth data available for assimilation. The main effect of the downscaling
257 is a better representation of the air temperature distribution and therefore a better representation of the solid precipitation
258 fraction. Then, the performance of the SnowModel simulated SWE largely relies on ERA5 precipitation. Our results suggest
259 that the winter precipitation is well represented by ERA5 over the Sierra Nevada, in agreement with previous studies
260 highlighting the good performances of ERA5 precipitation especially in extratropical regions (Lavers et al., 2022). We find an
261 overestimation of snow accumulation in high elevation which occurs only above 3000 m asl. In the study domain, the maximum
262 elevation of ERA5 and ERA5-Land grid cells are 2654 m and 3100 m respectively. Hence the overestimation shown in Figure
263 5 is most probably due to the extrapolation of ERA5 precipitation by MicroMet. MicroMet uses monthly coefficients to adjust
264 precipitation with elevation. These coefficients were derived from a large precipitation gauge dataset in the Western North
265 America including the Tuolumne river catchment (Liston and Elder, 2006b). As a result, they only represent a first order
266 variation of precipitation with elevation and may introduce large biases only in areas whose fine scale elevation (i.e. at the
267 scale of the 100 m grid) deviates substantially from the ERA5 grid cell elevation. A possible source of error in high elevation
268 regions is the lack of gravitational transport in SnowModel. High elevation and steep slopes are prone to avalanches thereby
269 reducing the accumulated snow in these areas during the winter season (Quéno et al., 2023). However, we did not find a clear
270 correlation between the terrain slope and the model error (Fig. 5). Slopes above 15% have a slightly wider error distribution
271 but the mean absolute biases remain below 0.10 m w.e for both simulations. We also verified the residuals distribution by
272 average slope classes computed from a 3 m resolution slope raster (computed from the ASO snow-off lidar DEM) and found
273 similar results. Hence, we do not see clear evidence that the lack of gravitational transport is the main cause of the high
274 elevation biases. Another significant source of uncertainty is related to the albedo parameterization in SnowModel. The
275 deposition of light absorbing particles like dust can reduce albedo and therefore increase melt especially at high elevation
276 (Skiles et al., 2018; Dumont et al., 2020). This might explain the relative increase of the SWE bias between the 1st of April
277 and the 27th of May at all elevations above 2500 m (Figure 5).

278
279 At catchment scale we do not find a clear difference between ERA5-SnowModel and ERA5-Land-SnowModel outputs. This
280 suggests that the details of the downscaling scheme are not the primary factors of the simulation performance. However, there
281 is a deviation between both simulations at high elevation. As shown in Figure 5, the downscaling of ERA5 creates a strictly
282 increasing bias with elevation above 2500 m, whereas ERA5-Land creates a more complex bias that is negative between 2000
283 m and 3000 m and becomes positive above 3500 m. This more complex bias distribution reflects the fact that the output of the
284 ERA5-Land SnowModel pipeline is the result of two downscaling schemes (first ERA5 to ERA5-Land, then ERA5-Land to
285 100 m using MicroMet, Fig. 2). ERA5-Land atmospheric variables are generated by linear interpolation of their ERA5
286 counterparts. ERA5-Land air temperature and humidity are also adjusted using the grid cell elevation using a daily lapse rate

287 derived from ERA5 lower troposphere temperature vertical profile (Dutra et al., 2020). This is similar to the MicroMet
288 algorithm. Yet, there are several differences. In particular, the air temperature downscaling scheme in ERA5-Land is based on
289 a daily environmental lapse rate derived from ERA5 lower troposphere temperature vertical profiles (Muñoz Sabater, 2019),
290 whereas MicroMet lapse rates are fixed by month. Unlike ERA5-Land, MicroMet also adjusts the precipitation rates using a
291 function of elevation (Liston and Elder, 2006b). This is the cause of the non-monotonic evolution of the SWE bias by elevation
292 from ERA5-Land-SnowModel. In future applications we will favor ERA5 instead of ERA5-Land to avoid conflicting
293 processes in the downscaling of atmospheric variables. It makes it easier to adjust the precipitation correction factors from
294 local data. Using ERA5 is also more practical as it significantly reduces the download time, computing cost and memory usage
295 of our pipeline.

296
297 In Figure 3, we note the very good performance of ERA5-Land SWE at catchment scale despite its coarse scale (9 km
298 resolution). This result is in line with Muñoz-Sabater et al. (2021) who find better performances of ERA5-Land than ERA5
299 between 1500 m and 3000 m a.s.l. because 68% of the Tuolumne River catchment is in this elevation band.. Shao et al. (2022)
300 found a great accuracy of the ERA5-Land SWE dataset with an RMSE below 0.04 m w.e. in regions north of 45°N. Overall,
301 the performance of ERA5-Land SWE needs to be consolidated in other regions and ideally over larger domains of mountainous
302 areas. Previous studies suggested that a resolution below 500 m is required to properly simulate the snowpack distribution
303 (Baba et al., 2019; Bair et al., 2023). In addition, ERA5-Land resolution does not meet the essential climate variable
304 requirements set by the World Meteorological Organization for SWE (goal is 500 m resolution) (WMO e-Library, 2024).

305
306 Regarding Sentinel-1, Figure 7 suggests that the snow depth is well captured by the C-SNOW algorithm at 1 km resolution.
307 Although we are interested in SWE and not snow depth, the ASO program has shown that useful SWE products can be derived
308 from remotely sensed snow depth when combined with in situ measurements and modelisation of snow density (Painter et al.,
309 2016). Figure 7 shows that Sentinel-1 snow depth dataset seems to represent quite accurately the spatial variability inside the
310 catchment, although we note a slight underestimation for all three dates before the melting period (2017 and 2019) and after it
311 (2018). There is no clear pattern in the errors that emerge from these three dates. The modeling approach with ERA-5 (Land)
312 and SnowModel yields similar performances in terms of snow depth as the C-SNOW product on the same dates. However,
313 two patterns appear on Figure 7 for these approaches. i) The simulations with ERA5 and SnowModel are mostly centered
314 around a negative bias constant with the observed snow depth before the melting period (2017 and 2019), probably representing
315 a small negative bias in the ERA5 precipitation. ii) The simulations with ERA5-Land SnowModel seem to cap at 4 m which
316 could be the result of the two consecutives downscaling in the precipitations : the combination of an underestimation of ERA5
317 precipitation and its downscaling, plus the limitation of the elevation difference between ERA5-Land stations and the DEM
318 so the MicroMet precipitation factor can not enhance enough the high resolution precipitations. There are different error
319 sources in the three methods which are neither insignificant nor prohibitive for an operational use. Overall, the key difference

320 is that the model provides temporally continuous SWE, snow depth and other relevant variables like snowmelt runoff, whereas
321 C-SNOW snow depth products are temporally sparse and often masked during the melt season.

322

323 Our study has several limitations. Despite the large amount of data that were used for this study, our analysis is biased towards
324 the melt season since most of the ASO surveys were performed during the melt season for operational purposes. As a
325 consequence, the evaluation of the Sentinel-1 snow depth is limited to three dates only. In addition, we used ASO SWE which
326 is not a direct observation but a combination of accurate snow depth measurements and modeled snow density. Previous work
327 has shown that SWE variability is mostly driven by the snow depth variability (López-Moreno et al., 2013; Sturm et al., 2010).
328 Another limitation is the fact that ERA5 meteorological forcings may not be homogeneous across the globe due to the uneven
329 distribution of the assimilated observations. In addition, MicroMet precipitation correction coefficients were obtained from a
330 large region covering the study area, hence they may not be applicable in other regions. Therefore, we cannot generalize our
331 results to other regions. However, the increasing weight of global satellite observations in ERA5 over time suggests that ERA5
332 performances should be more spatially homogeneous in the recent and upcoming years. As a consequence, ERA5 uncertainty
333 varies with time since more and more data are available for data assimilation (Bell et al., 2021). This could be a limitation to
334 compute trends over large periods (Bengtsson et al., 2004).

335

336 However these errors have a low impact at the catchment scale and we can conclude that ERA5-SnowModel is promising for
337 water resources applications. This pipeline can be used to simulate SWE in near real time without the need of in situ
338 measurements. The development of a parallel version of SnowModel opens the door to continental scale applications (Mower
339 et al., 2023).

340 **5 Conclusion**

341 We have evaluated a pipeline to simulate the snowpack in mountainous catchment from global datasets only. This tool is based
342 on Copernicus land cover and DEM, ERA5 (or ERA5-Land) and SnowModel. It uses SnowModel/MicroMet to downscale
343 meteorological variables from ERA5 before computing accumulation and ablation processes using other SnowModel
344 submodels. It can generate daily gridded snow water equivalent over any region and any period of interest since 1940. Based
345 on 49 reference SWE surveys spanning seven contrasted hydrological years, we find that the ERA5-SnowModel combination
346 simulates well the SWE at the scale of the Tuolumne river catchment, with RMSE of 0.06 m (and 0.08 m with ERA5-Land)
347 and correlation of 0.99 (with both datasets). The SWE is also well simulated by elevation bands, except in the highest elevation
348 band where unrealistic SWE values were simulated. Between ERA5 and ERA5-Land, ERA5 is more convenient to use
349 especially because it requires less computing resources. Using the near real time release of ERA5 allows the simulation of
350 SWE with a 5 day latency. This makes this method usable in operational context and competitive with a satellite-based

351 approach. In particular, we found that it simulates the snow depth as well as the C-SNOW products derived from Sentinel-1,
352 which is only available during dry snow conditions.

353

354 Our study focused on a single catchment due to the availability of the ASO SWE products. However, ERA5 skills may vary
355 geographically and temporally due to the heterogeneity of assimilated data sources. Therefore, the performance of this method
356 should be evaluated in other mountain catchments. Recent remote sensing methods to retrieve snow depth from very high
357 resolution stereoscopic imagery will be useful for that perspective. To further reduce the errors in the simulation at finer
358 resolution, we also intend to add a data assimilation module in order to take advantage of other global datasets such as the
359 snow cover area from remote sensing.

360 **Competing Interest**

361 Co-authors KB was a member of the NASA ASO team (which produced the lidar data used in this study). KB is currently
362 employed by ASO, Inc., formed as a result of the ASO NASA technology transition effort.

363 **Acknowledgements**

364 We sincerely thank G. Liston for sharing the SnowModel code. We thank Franziska Koch and Olivier Merlin for fruitful
365 discussions about this work.

366

367 **Code Availability**

368 The wrapper around the SnowModel code can be found here : SOURP Laura / ERA_SnowModel_Pipeline · GitLab:
369 https://src.koda.cnrs.fr/laura.sourp.1/era_snowmodel_pipeline, last access: 15 March 2024.

370 **References**

371 Copernicus Digital Elevation Model: <https://spacedata.copernicus.eu/collections/copernicus-digital-elevation-model>, last
372 access: 9 October 2023.

373 Retrieving data — Climate Data Store Toolbox 1.1.5 documentation: [https://cds.climate.copernicus.eu/toolbox/doc/how-](https://cds.climate.copernicus.eu/toolbox/doc/how-to/1_how_to_retrieve_data/1_how_to_retrieve_data.html)
374 [to/1_how_to_retrieve_data/1_how_to_retrieve_data.html](https://cds.climate.copernicus.eu/toolbox/doc/how-to/1_how_to_retrieve_data/1_how_to_retrieve_data.html), last access: 27 June 2024.

375 Armstrong, R. L., Rittger, K., Brodzik, M. J., Racoviteanu, A., Barrett, A. P., Khalsa, S.-J. S., Raup, B., Hill, A. F., Khan, A.
376 L., Wilson, A. M., Kayastha, R. B., Fetterer, F., and Armstrong, B.: Runoff from glacier ice and seasonal snow in High Asia:
377 separating melt water sources in river flow, Reg. Environ. Change, <https://doi.org/10.1007/s10113-018-1429-0>, 2018.

378 Baba, M. W., Gascoïn, S., Jarlan, L., Simonneaux, V., and Hanich, L.: Variations of the Snow Water Equivalent in the Ourika
379 Catchment (Morocco) over 2000–2018 Using Downscaled MERRA-2 Data, *Water*, 10, 1120,
380 <https://doi.org/10.3390/w10091120>, 2018.

381 Baba, M. W., Gascoïn, S., Kinnard, C., Marchane, A., and Hanich, L.: Effect of Digital Elevation Model Resolution on the
382 Simulation of the Snow Cover Evolution in the High Atlas, *Water Resour. Res.*, 55, 5360–5378,
383 <https://doi.org/10.1029/2018WR023789>, 2019.

384 Baba, M. W., Boudhar, A., Gascoïn, S., Hanich, L., Marchane, A., and Chehbouni, A.: Assessment of MERRA-2 and ERA5
385 to Model the Snow Water Equivalent in the High Atlas (1981–2019), *Water*, 13, 890, <https://doi.org/10.3390/w13070890>,
386 2021.

387 Bair, E. H., Dozier, J., Rittger, K., Stilling, T., Kleiber, W., and Davis, R. E.: How do tradeoffs in satellite spatial and
388 temporal resolution impact snow water equivalent reconstruction?, *The Cryosphere*, 17, 2629–2643, [https://doi.org/10.5194/tc-](https://doi.org/10.5194/tc-17-2629-2023)
389 [17-2629-2023](https://doi.org/10.5194/tc-17-2629-2023), 2023.

390 Bell, B., Hersbach, H., Simmons, A., Berrisford, P., Dahlgren, P., Horányi, A., Muñoz-Sabater, J., Nicolas, J., Radu, R.,
391 Schepers, D., Soci, C., Villaume, S., Bidlot, J.-R., Haimberger, L., Woollen, J., Buontempo, C., and Thépaut, J.-N.: The ERA5
392 global reanalysis: Preliminary extension to 1950, *Q. J. R. Meteorol. Soc.*, 147, 4186–4227, <https://doi.org/10.1002/qj.4174>,
393 2021.

394 Bengtsson, L., Hagemann, S., and Hodges, K. I.: Can climate trends be calculated from reanalysis data?, *J. Geophys. Res.*
395 *Atmospheres*, 109, <https://doi.org/10.1029/2004JD004536>, 2004.

396 Billecocq, P., Langlois, A., and Montpetit, B.: Subgridding High Resolution Numerical Weather Forecast in the Canadian
397 Selkirk range for local snow modelling in a remote sensing perspective, *EGUsphere*, 1–24, [https://doi.org/10.5194/egusphere-](https://doi.org/10.5194/egusphere-2023-1152)
398 [2023-1152](https://doi.org/10.5194/egusphere-2023-1152), 2023.

399 Bormann, K. J., Westra, S., Evans, J. P., and McCabe, M. F.: Spatial and temporal variability in seasonal snow density, *J.*
400 *Hydrol.*, 484, 63–73, <https://doi.org/10.1016/j.jhydrol.2013.01.032>, 2013.

401 Buchhorn, M., Smets, B., Bertels, L., Roo, B. D., Lesiv, M., Tsendbazar, N.-E., Herold, M., and Fritz, S.: Copernicus Global
402 Land Service: Land Cover 100m: collection 3: epoch 2019: Globe (V3.0.1), <https://doi.org/10.5281/zenodo.3939050>, 2020.

403 Buck, A. L.: New Equations for Computing Vapor Pressure and Enhancement Factor, *J. Appl. Meteorol. Climatol.*, 20, 1527–
404 1532, [https://doi.org/10.1175/1520-0450\(1981\)020<1527:NEFCVP>2.0.CO;2](https://doi.org/10.1175/1520-0450(1981)020<1527:NEFCVP>2.0.CO;2), 1981.

405 Deschamps-Berger, C., Gascoïn, S., Shean, D., Besso, H., Guiot, A., and López-Moreno, J. I.: Evaluation of snow depth
406 retrievals from ICESat-2 using airborne laser-scanning data, *The Cryosphere*, 17, 2779–2792, [https://doi.org/10.5194/tc-17-](https://doi.org/10.5194/tc-17-2779-2023)
407 [2779-2023](https://doi.org/10.5194/tc-17-2779-2023), 2023.

408 Dumont, M., Tuzet, F., Gascoïn, S., Picard, G., Kutuzov, S., Lafaysse, M., Cluzet, B., Nheili, R., and Painter, T. H.: Accelerated
409 Snow Melt in the Russian Caucasus Mountains After the Saharan Dust Outbreak in March 2018, *Journal of Geophysical*
410 *Research: Earth Surface*, 125, <https://doi.org/10.1029/2020JF005641>, 2020.

411 Dutra, E., Muñoz-Sabater, J., Boussetta, S., Komori, T., Hirahara, S., and Balsamo, G.: Environmental Lapse Rate for High-
412 Resolution Land Surface Downscaling: An Application to ERA5, *Earth Space Sci.*, 7, e2019EA000984,
413 <https://doi.org/10.1029/2019EA000984>, 2020.

414 Fayad, A., Gascoin, S., Faour, G., López-Moreno, J. I., Drapeau, L., Page, M. L., and Escadafal, R.: Snow hydrology in
415 Mediterranean mountain regions: A review, *J. Hydrol.*, 551, 374–396, <https://doi.org/10.1016/j.jhydrol.2017.05.063>, 2017.

416 Freudiger, D., Kohn, I., Seibert, J., Stahl, K., and Weiler, M.: Snow redistribution for the hydrological modeling of alpine
417 catchments, *Wiley Interdiscip. Rev. Water*, 4, e1232, <https://doi.org/10.1002/wat2.1232>, 2017.

418 GDAL/OGR contributors: GDAL/OGR Geospatial Data Abstraction software Library, Open Source Geospatial Foundation,
419 <https://doi.org/10.5281/zenodo.5884351>, 2024.

420 Griffin, D. and Anchukaitis, K. J.: How unusual is the 2012–2014 California drought?, *Geophys. Res. Lett.*, 41, 9017–9023,
421 <https://doi.org/10.1002/2014GL062433>, 2014.

422 Günther, D., Marke, T., Essery, R., and Strasser, U.: Uncertainties in Snowpack Simulations—Assessing the Impact of Model
423 Structure, Parameter Choice, and Forcing Data Error on Point-Scale Energy Balance Snow Model Performance, *Water Resour.*
424 *Res.*, 55, 2779–2800, <https://doi.org/10.1029/2018WR023403>, 2019.

425 Guyennon, N., Valt, M., Salerno, F., Petrangeli, A. B., and Romano, E.: Estimating the snow water equivalent from snow
426 depth measurements in the Italian Alps, *Cold Reg. Sci. Technol.*, 167, 102859,
427 <https://doi.org/10.1016/j.coldregions.2019.102859>, 2019.

428 Hersbach, H., Bell, B., Berrisford, P., Hirahara, S., Horányi, A., Muñoz-Sabater, J., Nicolas, J., Peubey, C., Radu, R., Schepers,
429 D., Simmons, A., Soci, C., Abdalla, S., Abellan, X., Balsamo, G., Bechtold, P., Biavati, G., Bidlot, J., Bonavita, M., De Chiara,
430 G., Dahlgren, P., Dee, D., Diamantakis, M., Dragani, R., Flemming, J., Forbes, R., Fuentes, M., Geer, A., Haimberger, L.,
431 Healy, S., Hogan, R. J., Hólm, E., Janisková, M., Keeley, S., Laloyaux, P., Lopez, P., Lupu, C., Radnoti, G., de Rosnay, P.,
432 Rozum, I., Vamborg, F., Villaume, S., and Thépaut, J.-N.: The ERA5 global reanalysis, *Q. J. R. Meteorol. Soc.*, 146, 1999–
433 2049, <https://doi.org/10.1002/qj.3803>, 2020.

434 Lievens, H., Demuzere, M., Marshall, H.-P., Reichle, R. H., Brucker, L., Brangers, I., de Rosnay, P., Dumont, M., Giroto, M.,
435 Immerzeel, W. W., Jonas, T., Kim, E. J., Koch, I., Marty, C., Saloranta, T., Schöber, J., and De Lannoy, G. J. M.: Snow depth
436 variability in the Northern Hemisphere mountains observed from space, *Nat. Commun.*, 10, 4629,
437 <https://doi.org/10.1038/s41467-019-12566-y>, 2019.

438 Lievens, H., Brangers, I., Marshall, H.-P., Jonas, T., Olefs, M., and De Lannoy, G.: Sentinel-1 snow depth retrieval at sub-
439 kilometer resolution over the European Alps, *The Cryosphere*, 16, 159–177, <https://doi.org/10.5194/tc-16-159-2022>, 2022.

440 Liston, G. E. and Elder, K.: A Distributed Snow-Evolution Modeling System (SnowModel), *J. Hydrometeorol.*, 7, 1259–1276,
441 <https://doi.org/10.1175/JHM548.1>, 2006a.

442 Liston, G. E. and Elder, K.: A Meteorological Distribution System for High-Resolution Terrestrial Modeling (MicroMet), *J.*
443 *Hydrometeorol.*, 7, 217–234, <https://doi.org/10.1175/JHM486.1>, 2006b.

444 Liston, G. E., Haehnel, R. B., Sturm, M., Hiemstra, C. A., Berezovskaya, S., and Tabler, R. D.: Simulating complex snow
445 distributions in windy environments using SnowTran-3D, *J. Glaciol.*, 53, 241–256,
446 <https://doi.org/10.3189/172756507782202865>, 2007.

447 Liston, G. E., Itkin, P., Stroeve, J., Tschudi, M., Stewart, J. S., Pedersen, S. H., Reinking, A. K., and Elder, K.: A Lagrangian
448 Snow-Evolution System for Sea-Ice Applications (SnowModel-LG): Part I—Model Description, *J. Geophys. Res. Oceans*,
449 125, e2019JC015913, <https://doi.org/10.1029/2019JC015913>, 2020.

450 Liu, Y., Fang, Y., Li, D., and Margulis, S. A.: How Well do Global Snow Products Characterize Snow Storage in High
451 Mountain Asia?, *Geophys. Res. Lett.*, 49, e2022GL100082, <https://doi.org/10.1029/2022GL100082>, 2022.

452 López-Moreno, J. I., Fassnacht, S. R., Heath, J. T., Musselman, K. N., Revuelto, J., Latron, J., Morán-Tejeda, E., and Jonas,
453 T.: Small scale spatial variability of snow density and depth over complex alpine terrain: Implications for estimating snow
454 water equivalent, *Adv. Water Resour.*, 55, 40–52, <https://doi.org/10.1016/j.advwatres.2012.08.010>, 2013.

455 Mankin, J. S., Viviroli, D., Singh, D., Hoekstra, A. Y., and Diffenbaugh, N. S.: The potential for snow to supply human water
456 demand in the present and future, *Environ. Res. Lett.*, 10, 114016, <https://doi.org/10.1088/1748-9326/10/11/114016>, 2015.

457 Marti, R., Gascoin, S., Berthier, E., de Pinel, M., Houet, T., and Laffly, D.: Mapping snow depth in open alpine terrain from
458 stereo satellite imagery, *The Cryosphere*, 10, 1361–1380, <https://doi.org/10.5194/tc-10-1361-2016>, 2016.

459 Mernild, S. H., Liston, G. E., Hiemstra, C. A., Malmros, J. K., Yde, J. C., and McPhee, J.: The Andes Cordillera. Part I: snow
460 distribution, properties, and trends (1979–2014), *Int. J. Climatol.*, 37, 1680–1698, <https://doi.org/10.1002/joc.4804>, 2017.

461 Mower, R., Gutmann, E. D., Lundquist, J., Liston, G. E., and Rasmussen, S.: Parallel SnowModel (v1.0): a parallel
462 implementation of a Distributed Snow-Evolution Modeling System (SnowModel), *EGUsphere*, 1–27,
463 <https://doi.org/10.5194/egusphere-2023-1612>, 2023.

464 Muñoz Sabater, J.: ERA5-Land hourly data from 1950 to present, <https://doi.org/10.24381/cds.e2161bac>, 2019.

465 Muñoz-Sabater, J., Dutra, E., Agustí-Panareda, A., Albergel, C., Arduini, G., Balsamo, G., Boussetta, S., Choulga, M.,
466 Harrigan, S., Hersbach, H., Martens, B., Miralles, D. G., Piles, M., Rodríguez-Fernández, N. J., Zsoter, E., Buontempo, C.,
467 and Thépaut, J.-N.: ERA5-Land: a state-of-the-art global reanalysis dataset for land applications, *Earth Syst. Sci. Data*, 13,
468 4349–4383, <https://doi.org/10.5194/essd-13-4349-2021>, 2021.

469 Painter, T. H., Berisford, D. F., Boardman, J. W., Bormann, K. J., Deems, J. S., Gehrke, F., Hedrick, A., Joyce, M., Laidlaw,
470 R., Marks, D., Mattmann, C., McGurk, B., Ramirez, P., Richardson, M., Skiles, S. M., Seidel, F. C., and Winstral, A.: The
471 Airborne Snow Observatory: Fusion of scanning lidar, imaging spectrometer, and physically-based modeling for mapping
472 snow water equivalent and snow albedo, *Remote Sens. Environ.*, 184, 139–152, <https://doi.org/10.1016/j.rse.2016.06.018>,
473 2016.

474 Painter, T. H., Bormann, K., Deems, J. S., Hedrick, A. R., Marks, D. G., Skiles, M., and Stock, G. M.: Through the Looking
475 Glass: Droughtorama to Snowpocalypse in the Sierra Nevada as studied with the NASA Airborne Snow Observatory, 2017,
476 C12C-08, 2017.

477 Quéno, L., Mott, R., Morin, P., Cluzet, B., Mazzotti, G., and Jonas, T.: Snow redistribution in an intermediate-complexity
478 snow hydrology modelling framework, *EGU*sphere, 1–32, <https://doi.org/10.5194/egusphere-2023-2071>, 2023.

479 Raleigh, M. S., Livneh, B., Lapo, K., and Lundquist, J. D.: How Does Availability of Meteorological Forcing Data Impact
480 Physically Based Snowpack Simulations?, *J. Hydrometeorol.*, 17, 99–120, <https://doi.org/10.1175/JHM-D-14-0235.1>, 2016.

481 Shao, D., Li, H., Wang, J., Hao, X., Che, T., and Ji, W.: Reconstruction of a daily gridded snow water equivalent product for
482 the land region above 45° N based on a ridge regression machine learning approach, *Earth Syst. Sci. Data*, 14, 795–809,
483 <https://doi.org/10.5194/essd-14-795-2022>, 2022.

484 Skiles, S. M., Flanner, M., Cook, J. M., Dumont, M., and Painter, T. H.: Radiative forcing by light-absorbing particles in snow,
485 *Nature Clim Change*, 8, 964–971, <https://doi.org/10.1038/s41558-018-0296-5>, 2018.

486 Sturm, M., Taras, B., Liston, G. E., Derksen, C., Jonas, T., and Lea, J.: Estimating Snow Water Equivalent Using Snow Depth
487 Data and Climate Classes, *J. Hydrometeorol.*, 11, 1380–1394, <https://doi.org/10.1175/2010JHM1202.1>, 2010.

488 Sturm, M., Goldstein, M. A., and Parr, C.: Water and life from snow: A trillion dollar science question: SNOW AND LIFE,
489 *Water Resour. Res.*, 53, 3534–3544, <https://doi.org/10.1002/2017WR020840>, 2017.

490 Tsai, Y.-L. S., Dietz, A., Oppelt, N., and Kuenzer, C.: Remote Sensing of Snow Cover Using Spaceborne SAR: A Review,
491 *Remote Sens.*, 11, 1456, <https://doi.org/10.3390/rs11121456>, 2019.

492 Urraca, R. and Gobron, N.: Temporal stability of long-term satellite and reanalysis products to monitor snow cover trends, *The*
493 *Cryosphere*, 17, 1023–1052, <https://doi.org/10.5194/tc-17-1023-2023>, 2023.

494 Viviroli, D., Kummu, M., Meybeck, M., Kallio, M., and Wada, Y.: Increasing dependence of lowland populations on mountain
495 water resources, *Nat. Sustain.*, 3, 917–928, <https://doi.org/10.1038/s41893-020-0559-9>, 2020.

496 Weber, M., Koch, F., Bernhardt, M., and Schulz, K.: The evaluation of the potential of global data products for snow
497 hydrological modelling in ungauged high-alpine catchments, *Hydrol. Earth Syst. Sci.*, 25, 2869–2894,
498 <https://doi.org/10.5194/hess-25-2869-2021>, 2021.

499 WMO e-Library: <https://library.wmo.int/idurl/4/58104>, last access: 15 March 2024.

500 Wrzesien, M. L., Pavelsky, T. M., Durand, M. T., Dozier, J., and Lundquist, J. D.: Characterizing Biases in Mountain Snow
501 Accumulation From Global Data Sets, *Water Resour. Res.*, 55, 9873–9891, <https://doi.org/10.1029/2019WR025350>, 2019.

502

503

Copernicus class number	Copernicus Vegetation type	Forest type	Leaf type	Chosen corresponding SM class	SM class number
0	Nodata				-9999
20	Shrubs			Mesic upland shrub	6
30	Herbaceous Vegetation			Grassland rangeland	12
40	cropland			short crops	23
50	Urban			Residential/urban	21
60	sparse vegetation			Bare	18
70	Snow and ice			Permanent snow/glacier	20
80	Permanent water bodies			water/ possibly frozen	19
90	Herbaceous wetland			Shrub wetland/ riparian	9
100	Moss and lichen			Bare	18
111	closed forest	evergreen	needle	Coniferous forest	1
112	closed forest	evergreen	broad	Coniferous forest	1
113	closed forest	deciduous	needle	Deciduous forest	2

114	closed forest	deciduous	broad	Deciduous forest	2
115	closed forest	mixed		Mixed forest	3
116	closed forest	unknown		Mixed forest	3
121	open forest	evergreen	needle	Coniferous forest	1
122	open forest	evergreen	broad	Coniferous forest	1
123	open forest	deciduous	needle	Deciduous forest	2
124	open forest	deciduous	broad	Deciduous forest	2
125	open forest	mixed		Mixed forest	3
126	open forest	unknown		Mixed forest	3
200	open sea			Ocean	24

505

506 **Table A1 : Correspondence table between Copernicus land cover and SnowModel vegetation classes**